The Journal of Physical Chemistry Letters

pubs.acs.org/JPCL Letter

Penta-BCN: A New Ternary Pentagonal Monolayer with Intrinsic Piezoelectricity

Kexian Zhao, Yaguang Guo, Yiheng Shen, Qian Wang,* Y. Kawazoe, and Puru Jena

Cite This: J. Phys. Chem. Lett. 2020, 11, 3501−3506 Read Online

ACCESS | Metrics & More | Article Recommendations

ABSTRACT: Going beyond conventional hexagonal sheets, pentagonal 2D structures are of current interest due to their novel properties and broad applications. Herein, for the first time, we study a ternary pentagonal BCN monolayer, penta-BCN, which exhibits intrinsic piezoelectric properties. Based on state-of-the-art theoretical calculations, we find that penta-BCN is stable mechanically, thermally, and dynamically and has a direct band gap of 2.81 eV. Due to its unique atomic configuration with noncentrosymmetric and semiconducting features, penta-BCN displays high spontaneous polarization of 3.17×10^{-10} C/m and a prominent piezoelectricity with $d_{21} = 0.878$ pm/V, $d_{22} = -0.678$ pm/V, and $d_{16} = 1.72$ pm/V, which are larger than those of an *h*-BN sheet and functionalized pentagraphene. Since B, C, and N are rich in resources, light in mass, and benign to the environment, the intrinsic polarization and piezoelectricity make the penta-BCN monolayer promising for technological applications. This study expands the family of 2D pentagonal structures with new features.

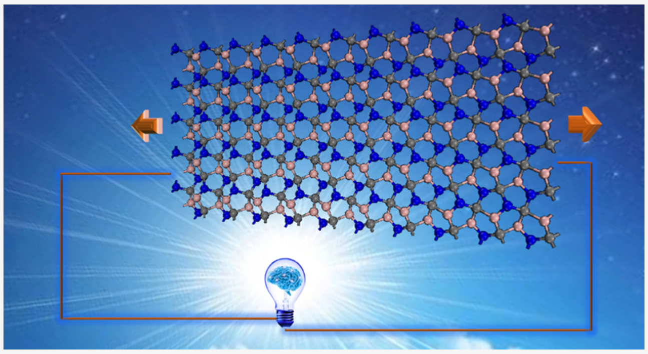

Since the theoretical prediction of pentagraphene (PG), a carbon allotrope purely composed of five-membered rings,[1] tremendous efforts have been made in recent years to rationally design and synthesize pentagon-based 2D materials with novel properties and promising applications. Many 2D nanosheets constructed exclusively from pentagon-based structural units have been proposed,[2−11] and some of them have been experimentally synthesized, including penta-$PdSe_2$[12−14] and pentasilicene nanoribbons.[15] These materials exhibit interesting electronic properties and have broad applications. For instance, a penta-CN_2 sheet[6] exhibits high energy density of 4.41 kJ/g, high in-plane axial Young's modulus of 319 N/m (even stiffer than a *h*-BN monolayer), and an interesting double degeneracy of its electronic band structure protected by nonsymmorphic symmetry. In addition, the penta-CN_2 sheet was also found to have a high lattice thermal conductivity of 660.71 W m^{-1} K^{-1} due to its unique geometry,[16] contrary to conventional wisdom that lone-pair electrons lead to low lattice thermal conductivity. Parallel to the study of a penta-CN_2 sheet, penta-CB_2[4] and penta-BN_2[5] were also systematically investigated; the former can be flexibly tuned from a semiconductor to a semimetal by strain, while the latter shows a negative Poisson's ratio and tunable electronic structure from semiconducting to metallic. These intriguing properties of pentasheets make them promising for vast applications. For example, an Ohmic contact between pentagraphene and graphene can be achieved by applying an electric field or doping the graphene sheet with N atoms.[17] A Schottky contact built by vertically stacking pentagraphene and penta-BN_2 can be tuned from *n*-type to *p*-type when the interlayer distance is changed.[18] Pentagraphene and penta-BN_2 have been found to be promising anode materials for Li-ion batteries.[11,19]

However, the design of nonmetal-element-based pentagonal 2D structures so far is limited to binary systems. We note that when going from unitary pentagraphene to binary pentastructures including penta-CB_2,[4] penta-BN_2,[5] and penta-CN_2,[6] the physical properties have been significantly enriched. Similarly, going from binary to ternary systems can offer more degrees of freedom to tune the physical properties. This motivated us to design a stable *ternary* pentasheet containing B, C, and N atoms, because they are neighbors in the periodic table with similar atomic radii but distinctive electronegativity. In addition, they have many advantages over other nonmetal elements. Using first-principles calculations, we found a stable ternary pentagonal sheet, penta-BCN, which exhibits novel properties, including spontaneous polarization and intrinsic piezoelectricity.

Received: March 14, 2020
Accepted: April 15, 2020
Published: April 15, 2020

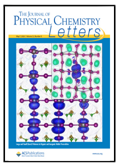

https://dx.doi.org/10.1021/acs.jpclett.0c00824
J. Phys. Chem. Lett. 2020, 11, 3501−3506

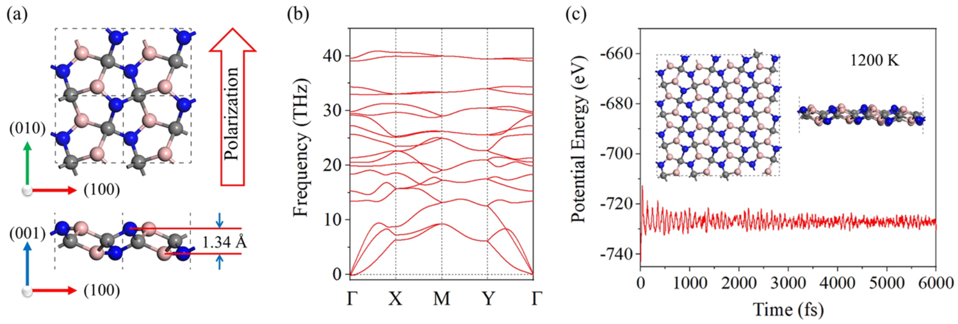

Figure 1. (a) Top and side views of the optimized structure, and (b) phonon band structure of penta-BCN. (c) Potential energy fluctuation of penta-BCN with time during the AIMD simulation at 1200 K. The insets are the top and side views of the geometrical structure at the end of simulation. The gray, pink, and blue spheres represent C, B, and N atoms, respectively.

The structural and electronic properties of the penta-BCN sheet are calculated using density functional theory (DFT) as implemented in the Vienna *Ab initio* Simulation Package (VASP).[20] The interactions between electrons and nuclei are treated within the projector augmented wave (PAW) method[21] with a kinetic cutoff energy of 600 eV. The electronic exchange-correlation potential energy is incorporated using the generalized gradient approximation due to Perdew−Burke−Ernzerhof (PBE).[22] The hybrid Heyd−Scuseria−Ernzerhof (HSE06) functional[23] is further used to achieve more accurate results of the electronic properties. A vacuum spacing of 20 Å along the direction perpendicular to the plane is included to avoid the interactions between two neighboring images. The criteria for total energy and forces are set to 10^{-4} eV and 10^{-2} eV/Å, respectively. The first Brillouin zone is sampled by a 9 × 9 × 1 *k*-point grid within the Monkhorst−Pack scheme.[24] A PHONOPY package[25] is used to calculate phonon spectra to confirm the dynamic stability, and *ab initio* molecular dynamics (AIMD) simulations are performed to confirm the thermal stability.[26]

The piezoelectric tensors and piezoelectric strain tensors are defined as

$$e_{ijk} = \frac{\partial P_i}{\partial \varepsilon_{jk}} = e_{ijk}^{\text{elc}} + e_{ijk}^{\text{ion}} \tag{1}$$

and

$$d_{ijk} = \frac{\partial P_i}{\partial \sigma_{jk}} = d_{ijk}^{\text{elc}} + d_{ijk}^{\text{ion}} \tag{2}$$

Here, P_i is the piezoelectric polarization, and ε_{jk} and σ_{jk} are strain and stress, respectively. The relaxed-ion piezoelectric tensors $e_{ijk}(d_{ijk})$ are obtained from the sum of ionic and electronic contributions with the fully relaxed ionic positions. The relaxed-ion coefficients are reliable and widely used, as they are consistent with experimental results.[27,28] Using the Voigt notation[29] and the mapping of indices (11 → 1, 22 → 2, 33 → 3, 23 → 4, 31 → 5, and 12 → 6), the values of d_{ij} can be derived from the equation

$$e_{ik} = d_{ij} C_{jk} \tag{3}$$

where piezoelectric tensors e_{ij} can be written as

$$e_{ij} = \begin{Bmatrix} e_{11} & e_{12} & \cdots & e_{16} \\ e_{21} & e_{22} & \cdots & e_{26} \\ e_{31} & e_{32} & \cdots & e_{36} \end{Bmatrix} \tag{4}$$

Specifically, for 2D materials, we only need to consider in-plane strain components.[30,31] Thus, the relationship among the elastic, piezoelectric stress, and strain tensors becomes

$$\begin{pmatrix} e_{11} & e_{12} & e_{16} \\ e_{21} & e_{22} & e_{26} \\ e_{31} & e_{32} & e_{36} \end{pmatrix} = \begin{pmatrix} d_{11} & d_{12} & d_{16} \\ d_{21} & d_{22} & d_{26} \\ d_{31} & d_{32} & d_{36} \end{pmatrix} \begin{pmatrix} C_{11} & C_{12} & C_{16} \\ C_{21} & C_{22} & C_{26} \\ C_{31} & C_{32} & C_{36} \end{pmatrix} \tag{5}$$

The elastic stiffness tensor C_{ij} and piezoelectric tensor e_{ijk} are calculated by using the finite difference method and density functional perturbation theory (DFPT) as implemented in the VASP package, respectively, which has been widely used in previous studies.[30−35]

We constructed an initial ternary pentagonal structure, penta-BCN, based on the atomic configuration of pentagraphene,[1] by alternately replacing the threefold-coordinated C atoms with B and N and keeping the positions of four-coordinated C atoms unchanged. The optimized geometry of penta-BCN is given in Figure 1(a), which shows that penta-BCN is composed of pure BCN pentagons. The relaxed 2D crystal structure possesses C2_2 symmetry (space group No. 4) with the lattice parameters a = 3.67 Å and b = 3.63 Å and a buckling height of 1.34 Å. The unit cell contains six atoms with a C/B/N ratio of 1:1:1, as denoted by dashed lines in Figure 1(a). In this structure, the B−N, C−N, and C−B bond lengths are 1.41, 1.51, and 1.62 Å, respectively. We note that the B−N bond length is shorter than that in *h*-BN (1.44 Å)[36] and penta-BN_2 (1.55 Å),[5] suggesting that the B−N covalent bond in penta-BCN is stronger than that in *h*-BN and penta-BN_2. We also note that the special arrangement of B−N bonds breaks the centrosymmetry of the geometry, which in turn would induce spontaneous polarization and piezoelectric effect.

To verify the dynamic stability of penta-BCN, we calculated its phonon dispersion. As shown in Figure 1(b), there are no imaginary modes in the entire Brillouin zone, confirming that the penta-BCN structure is dynamically stable. To examine the thermal stability of penta-BCN, we further carried out AIMD simulations by using a 4 × 4 × 1 supercell for 6 ps with a time step of 1 fs for each simulation from 300 to 1200 K. We find that the structure remains intact at the end of the simulation and does not suffer significant distortion at 300 K. The total potential energy fluctuates slightly around a constant value during the simulation at 1200 K. The corresponding simulation results are plotted in Figure 1(c), which shows that penta-BCN is thermally stable even at a high temperature of 1200 K.

To study the mechanical stability and mechanical properties of penta-BCN, we calculated the linear elastic constants by

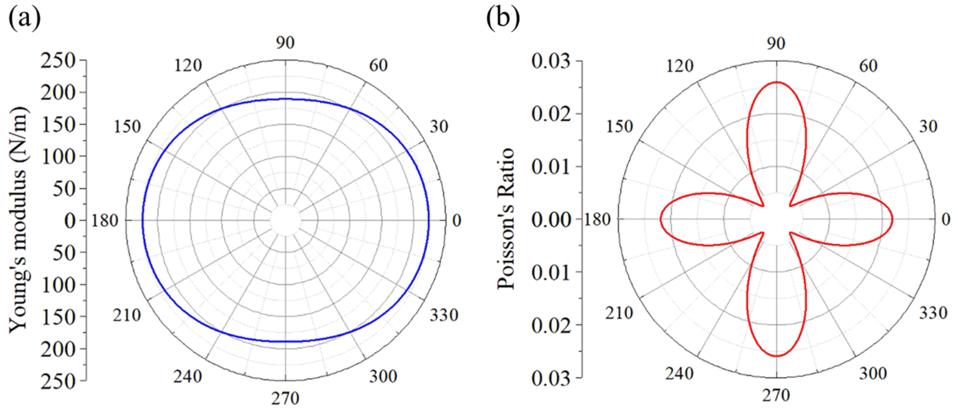

Figure 2. Variation of the (a) in-plane Young's modulus and (b) Poisson's ratio of penta-BCN with the crystal orientation of penta-BCN.

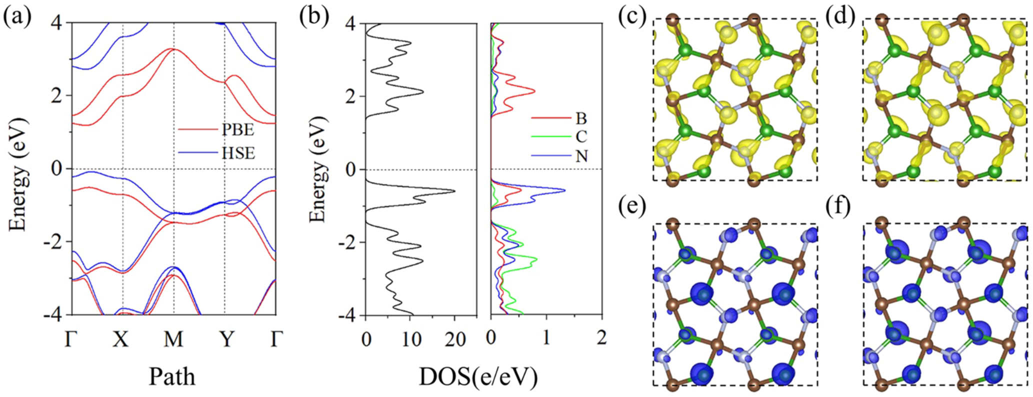

Figure 3. (a) Band structure of penta-BCN at the PBE and HSE06 levels, and (b) total and partial DOS at the PBE level. Band-decomposed charge density distribution of (c) the second highest valence band, (d) the VBM, (e) the CBM, and (f) the second lowest conduction band of penta-BCN.

using the finite distortion method.[37] The calculated elastic constants are C_{11} = 223.56 N/m, C_{22} = 189.16 N/m, $C_{12} = C_{21}$ = 4.90 N/m, and C_{66} = 104.88 N/m. According to Born–Huang criteria,[38] the elastic constants of penta-BCN satisfy $C_{11}C_{12} - C_{12}^2 > 0$ and $C_{66} > 0$, confirming that the penta-BCN monolayer is mechanically stable. The in-plane Young's moduli along the (100) and (010) directions (E_a and E_b) are derived from the formulas: $E_a = (C_{11}^2 - C_{12}^2)/C_{11}$ and $E_b = (C_{22}^2 - C_{21}^2)/C_{22}$; their corresponding values are 223.45 and 189.03 N/m, respectively. Note that these values are much larger than those of the MoS_2 monolayer (120 N/m),[39] suggesting that the penta-BCN sheet is even stiffer for curling. The Poisson's ratios are calculated to be ν_a = 0.022 and ν_b = 0.026, along the (100) and (010) directions, respectively. The different mechanical properties in the different directions indicate a mechanical anisotropy of penta-BCN.

To further explore the dependence of mechanical properties on the crystal orientation of penta-BCN, the tensor rotation matrix **T** is applied to calculate the stiffness tensor **C** by using the equation

$$\mathbf{C}' = \mathbf{T}^{-1}\cdot\mathbf{C}\cdot\mathbf{R}\cdot\mathbf{T}\cdot\mathbf{R}^{-1} \qquad (6)$$

where **R** = diag(1, 1, 2) is the bridge between the engineered strain and tensor strain. The calculated results are plotted in Figure 2. One can see that the maximum in-plane Young's modulus is located along the (100) direction (0°), and the minimum is along the (010) direction (90°). The maximum and minimum Poisson's Ratios are located along the (010) direction (90°) and near (110) direction (~45°) with values of 0.026 and 0.004, respectively, once again showing a high mechanical anisotropy of penta-BCN.

To study the electronic properties of penta-BCN, we calculated its band structure using the PBE and HSE06 functional as shown in Figure 3(a) in red and blue lines, respectively. One can see that penta-BCN is semiconducting with a direct bandgap of 1.70 eV at the PBE level, as both the valence band maximum (VBM) and conduction band minimum (CBM) are located at the same point along the Γ-X path in the first Brillouin zone. At the HSE06 level, the band structure has a similar dispersion but with a larger band gap of 2.81 eV due to the well-known fact that the PBE functional underestimates the band gaps of materials. To further analyze the electronic properties of penta-BCN, the total density of states (DOS) and partial DOS (PDOS) are calculated and plotted in Figure 3(b). From the PDOS, one can see that the VBM is mainly contributed by both B and N atoms, while the CBM dominantly comes from the B atoms. The contributions to the electronic states can also be seen from the band-decomposed charge density distributions, as shown in Figure 3(c–f). In addition, we note that the charge densities are asymmetrically distributed, implying that spontaneous polarization can exist in penta-BCN, which may lead to potential application in piezoelectrics.

To possess spontaneous electric polarization in 2D materials, it is necessary to have polarized bonds arranged in a noncentrosymmetric configuration. For pentagonal structures, such as PG and penta-CN_2, the biggest challenge in inducing polar states is that the sp^2 hybridized atoms are equivalent, where the positive and negative charge centers cannot be effectively separated due to the nonpolar bonds. To this end, we proposed that a small tilt of Si dimers can lead to ferroelectricity in a pentasilicene sheet, in which the polar bonds result from the inequivalent sp^2 Si atoms.[40] However, a more intuitive way is to use two different elements to replace the dimers. This is the case with penta-BCN, where one can see that the B−N bond is intrinsically polarized, differing from the sp^2 hybridized C−C in PG and N−N in penta-CN_2. Therefore, electric polarization can survive in this penta-BCN sheet. To quantify the spontaneous polarization of penta-BCN, we use the finite electric field method based on the Berry phase theory[41,42] to calculate the dipole moment. The total polarization P_s is determined by the sum of the ionic contribution P_s^{ion} and electronic contribution P_s^{ele}

$$P_s = P_s^{\text{ion}} + P_s^{\text{ele}} \tag{7}$$

The ionic contribution can be simply described as

$$P_s^{\text{ion}} = \frac{|e|}{\Omega} \sum_{i=1}^{N_{\text{atom}}} Z_i^{\text{V}} \Delta r_i \tag{8}$$

where e, Ω, N_{atom}, $|e|$, Z_i^{V},and Δr_i represent the electron charge, volume of the unit cell, number of atoms in the unit cell, valence charge of the i-th atom, and the displacement of i-th atom, respectively. The electronic contribution P_s^{ele} can be derived using the Berry phase approach. We find that the polarization P_s of penta-BCN is along the (010) direction, namely the direction parallel to the B−N bonds, while that along the (100) direction cancels each other out. The value of P_s is calculated to be 3.17×10^{-10} C/m, which is larger than that of h-BN (2.174×10^{-10} C/m),[43] because penta-BCN has a stronger B−N bond. Here, we find that the dipole in penta-BCN is permanent, i.e., it is difficult to change the direction of the dipole moment. Thus, penta-BCN can be considered as a pyroelectric material instead of a ferroelectric one.

We next study the piezoelectricity of penta-BCN as a pyroelectric material, which also exhibits a piezoelectric effect. The piezoelectric tensors for this 2D structure with C2_2 symmetry can be written as

$$e_{ij} = \left\{ \begin{matrix} 0 & 0 & 0 & e_{14} & 0 & e_{16} \\ e_{21} & e_{22} & e_{23} & 0 & e_{25} & 0 \\ 0 & 0 & 0 & e_{34} & 0 & e_{36} \end{matrix} \right\} \tag{9}$$

According to eq 5, the relationship among the elastic, piezoelectric stress, and strain tensors becomes

$$\begin{pmatrix} 0 & 0 & e_{16} \\ e_{21} & e_{22} & 0 \\ 0 & 0 & e_{36} \end{pmatrix} = \begin{pmatrix} 0 & 0 & d_{16} \\ d_{21} & d_{22} & 0 \\ 0 & 0 & d_{36} \end{pmatrix} \begin{pmatrix} C_{11} & C_{12} & C_{16} \\ C_{21} & C_{22} & C_{26} \\ C_{31} & C_{32} & C_{36} \end{pmatrix} \tag{10}$$

The d_{16}, d_{21}, d_{22}, and d_{36} are derived as

$$d_{16} = \frac{e_{16}}{C_{66}} \tag{11}$$

$$d_{21} = \frac{C_{21}e_{22} - C_{22}e_{21}}{C_{21}C_{12} - C_{11}C_{22}} \tag{12}$$

$$d_{22} = \frac{C_{12}e_{21} - C_{11}e_{22}}{C_{21}C_{12} - C_{11}C_{22}} \tag{13}$$

$$d_{36} = \frac{e_{36}}{C_{66}} \tag{14}$$

The calculated elastic stiffness coefficients C_{jk} along the polarization direction (010) and piezoelectric stress tensors e_{ik} are listed in Table 1. According to eqs 11−14, the piezoelectric strain tensors d_{ij} are derived from C_{jk} and e_{ik}, resulting in d_{21} = 0.878 pm/V, d_{22} = −0.678 pm/V, d_{16} = 1.72 pm/V, and d_{36} = −0.076 pm/V. For comparison, we list piezoelectric coefficients e and d for h-BN[27] and H-PG-G[44] in Table 2.

Table 1. Elastic Stiffness Coefficients C_{jk}, Piezoelectric Stress Tensors e_{ik}, and Piezoelectric Strain Tensors d_{ij} of Penta-BCN

C_{jk} (N/m)	C_{11}	C_{12}=C_{21}	C_{22}	C_{66}
	223.5	4.9	189.16	104.88
e_{ik} (10^{-10} C/m)	e_{21}	e_{22}	e_{16}	e_{36}
	1.93	−1.24	1.80	−0.08
d_{ij} (pm/V)	d_{21}	d_{22}	d_{16}	d_{36}
	0.878	−0.678	1.72	−0.076

Table 2. Piezoelectric Coefficients e and d for Some 2D Materials

material	e (10^{-10} C/m)	d (pm/V)
penta-BCN	1.93 (e_{21}), 1.80 (e_{16})	0.878 (d_{21}), 1.72 (d_{16})
h-BN[27]	1.38 (e_{11})	0.60 (d_{11})
H-PG-F[44]	0.97 (e_{31})	0.69 (d_{31})

We note that the d_{21} and d_{16} of penta-BCN are higher than the d_{11} of h-BN and d_{31} of H-PG-F. Usually, the softer the material, the larger the d coefficient.[45] Though the piezoelectric stress tensor e of penta-BCN is comparable to that of h-BN, its piezoelectric strain tensor d is larger, because penta-BCN possesses smaller elastic constants C. While in the functionalized pentagraphene sheet,[44] the polarization comes from the inequivalence of the H- and F-terminated surfaces. However, the small thickness of such a 2D sheet inhibits the full spatial separation of positive and negative charges, so the in-plane strain can hardly cause a significant change in polarization. This is why penta-BCN has a larger piezoelectric stress tensor e than that of H-PG-F. In addition, it is worth mentioning that the graphene-like BCN (h-BCN) monolayer has been synthesized recently,[46,47] where the $B_2C_2N_2$ (BCNBCN) hexagons are arranged antiparallel in a trigonal configuration.-Thus, the preserved inversion symmetry hinders the form of electric dipole and piezoelectricity in such a structure. From above, one can see that penta-BCN shows advantages in piezoelectricity as compared to some other nonmetal-element-based 2D materials, suggesting that penta-BCN could be an ideal candidate for piezoelectric materials with robust electromechanical coupling.

In summary, we have proposed a new ternary pentagonal sheet, penta-BCN, which is purely composed of BCN pentagons. By performing first-principles calculations combined with AIMD simulations, we have shown that penta-BCN is dynamically, thermally, and mechanically stable and is semiconducting with a direct band gap of 2.81 eV. The calculated Young's modulus and Poisson's ratio reveal that penta-BCN is mechanically anisotropic. The special arrangement of B−N bonds in this structure induces spontaneous polarization along the (010) direction with the magnitude of P_s

= 3.17×10^{-10} C/m, which is larger than that of *h*-BN because of the shorter B—N bond length. With noncentrosymmetric and semiconducting chrachteristics, penta-BCN exhibits piezoelectricity with d_{21} = 0.878 pm/V, d_{22} = −0.678 pm/V, and d_{16} = 1.72 pm/V, which are of the same order of magnitude as TMD materials and are larger than those in *h*-BN and hydrofluorinated PG. The spontaneous polarization and intrinsic piezoelectricity provide penta-BCN with great potential for a piezoelectric material at the nanoscale.

AUTHOR INFORMATION

Corresponding Author

Qian Wang − *Center for Applied Physics and Technology, Department of Materials Science and Engineering, HEDPS, BKL-MEMD, College of Engineering, Peking University, Beijing 100871, China*; orcid.org/0000-0002-9766-4617; Email: qianwang@pku.edu.cn

Authors

Kexian Zhao − *Center for Applied Physics and Technology, Department of Materials Science and Engineering, HEDPS, BKL-MEMD, College of Engineering, Peking University, Beijing 100871, China*

Yaguang Guo − *Center for Applied Physics and Technology, Department of Materials Science and Engineering, HEDPS, BKL-MEMD, College of Engineering, Peking University, Beijing 100871, China*

Yiheng Shen − *Center for Applied Physics and Technology, Department of Materials Science and Engineering, HEDPS, BKL-MEMD, College of Engineering, Peking University, Beijing 100871, China*

Y. Kawazoe − *New Industry Creation Hatchery Center, Tohoku University, Sendai 980-8577, Japan; Department of Physics, Suranaree University of Technology, 30000 Nakhon Ratchasima, Thailand; Department of Physics and Nanotechnology, SRM Institute of Science and Technology, Kattankulathur, Tamil Nadu 603203, India*

Puru Jena − *Department of Physics, Virginia Commonwealth University, Richmond, Virginia 23284, United States*; orcid.org/0000-0002-2316-859X

Complete contact information is available at:
https://pubs.acs.org/10.1021/acs.jpclett.0c00824

Notes

The authors declare no competing financial interest.

ACKNOWLEDGMENTS

This work is partially supported by grants from the National Natural Science Foundation of China (Grant Nos. 21773004 and 11974028), the National Key Research and Development Program of the Ministry of Science and Technology of China (Grant Nos. 2016YFE0127300 and 2017YFA0205003), and is supported by the High Performance Computing Platform of Peking University, China. Y.G. acknowledges the project funding by China Postdoctoral Science Foundation (No. 2019M650289). Y.K. acknowledges the financial support from JSPS Kakenhi Grant No. 17H03384 and HPCI project hp190111. P.J. acknowledges support by the U.S DOE, Office of Basic Energy Sciences, Division of Material Sciences and Engineering under Award No. DE-FG02-96ER45579. The authors thank the crew of the Center for Computational Materials Science, the Institute for Materials Research, Tohoku University (Japan), for their continuous support of the MASAMUNE-IMR supercomputing facility.

REFERENCES

(1) Zhang, S. H.; Zhou, J.; Wang, Q.; Chen, X. S.; Kawazoe, Y.; Jena, P. Penta-graphene: A new carbon allotrope. *Proc. Natl. Acad. Sci. U. S. A.* **2015**, *112* (8), 2372−2377.

(2) Li, X.; Dai, Y.; Li, M.; Wei, W.; Huang, B. Stable Si-based pentagonal monolayers: high carrier mobilities and applications in photocatalytic water splitting. *J. Mater. Chem. A* **2015**, 3 (47), 24055−24063.

(3) Ding, Y.; Wang, Y. Hydrogen-induced stabilization and tunable electronic structures of penta-silicene: a computational study. *J. Mater. Chem. C* **2015**, *3* (43), 11341−11348.

(4) Li, F.; Tu, K.; Zhang, H.; Chen, Z. Flexible structural and electronic properties of a pentagonal B_2C monolayer via external strain: a computational investigation. *Phys. Chem. Chem. Phys.* **2015**, *17* (37), 24151−24156.

(5) Li, J.; Fan, X.; Wei, Y.; Chen, G. Penta-B_xN_y sheet: A density functional theory study of two-dimensional material. *Sci. Rep.* **2016**, *6*, 31840.

(6) Zhang, S.; Zhou, J.; Wang, Q.; Jena, P. Beyond graphitic carbon nitride: Nitrogen-rich penta-CN_2 sheet. *J. Phys. Chem. C* **2016**, *120* (7), 3993−3998.

(7) Shojaei, F.; Hahn, J. R.; Kang, H. S. Electronic structure and photocatalytic band offset of few-layer GeP_2. *J. Mater. Chem. A* **2017**, *5* (42), 22146−22155.

(8) Zhao, J.; Zeng, H. Chemical Functionalization of Pentagermanene Leads to Stabilization and Tunable Electronic Properties by External Tensile Strain. *ACS Omega* **2017**, *2* (1), 171−180.

(9) Liu, L.; Kankam, I.; Zhuang, H. L. Single-layer antiferromagnetic semiconductor CoS_2 with pentagonal structure. *Phys. Rev. B: Condens. Matter Mater. Phys.* **2018**, *98* (20), 205425.

(10) Sun, S.; Meng, F.; Xu, Y.; He, J.; Ni, Y.; Wang, H. Flexible, auxetic and strain-tunable two dimensional penta-X_2C family as water splitting photocatalysts with high carrier mobility. *J. Mater. Chem. A* **2019**, *7* (13), 7791−7799.

(11) Zhang, T.; Ma, Y.; Huang, B.; Dai, Y. Two-Dimensional Penta-BN_2 with High Specific Capacity for Li-Ion Batteries. *ACS Appl. Mater. Interfaces* **2019**, *11* (6), 6104−6110.

(12) Oyedele, A. D.; Yang, S.; Liang, L.; Puretzky, A. A.; Wang, K.; Zhang, J.; Yu, P.; Pudasaini, P. R.; Ghosh, A. W.; Liu, Z.; et al. $PdSe_2$: Pentagonal two-dimensional layers with high air stability for electronics. *J. Am. Chem. Soc.* **2017**, *139* (40), 14090−14097.

(13) Chow, W. L.; Yu, P.; Liu, F.; Hong, J.; Wang, X.; Zeng, Q.; Hsu, C. H.; Zhu, C.; Zhou, J.; Wang, X.; et al. High Mobility 2D Palladium Diselenide Field-Effect Transistors with Tunable Ambipolar Characteristics. *Adv. Mater.* **2017**, *29* (21), 1602969.

(14) Li, E.; Wang, D.; Fan, P.; Zhang, R.; Zhang, Y.-Y.; Li, G.; Mao, J.; Wang, Y.; Lin, X.; Du, S.; et al. Construction of bilayer $PdSe_2$ on epitaxial graphene. *Nano Res.* **2018**, *11* (11), 5858−5865.

(15) Cerda, J. I.; Slawinska, J.; Le Lay, G.; Marele, A. C.; Gomez-Rodriguez, J. M.; Davila, M. E. Unveiling the pentagonal nature of perfectly aligned single-and double-strand Si nano-ribbons on Ag(110). *Nat. Commun.* **2016**, *7*, 13076.

(16) Wang, H.; Qin, G.; Qin, Z.; Li, G.; Wang, Q.; Hu, M. Lone-Pair Electrons Do Not Necessarily Lead to Low Lattice Thermal Conductivity: An Exception of Two-Dimensional Penta-CN_2. *J. Phys. Chem. Lett.* **2018**, *9* (10), 2474−2483.

(17) Guo, Y. G.; Wang, F. Q.; Wang, Q. An all-carbon vdW heterojunction composed of penta-graphene and graphene: Tuning the Schottky barrier by electrostatic gating or nitrogen doping. *Appl. Phys. Lett.* **2017**, *111* (7), No. 073503.

(18) Zhao, K.; Guo, Y.; Wang, Q. Contact properties of a vdW heterostructure composed of penta-graphene and penta-BN_2 sheets. *J. Appl. Phys.* **2018**, *124* (16), 165103.

(19) Xiao, B.; Li, Y. C.; Yu, X. F.; Cheng, J. B. Penta-graphene: A Promising Anode Material as the Li/Na-Ion Battery with Both

Extremely High Theoretical Capacity and Fast Charge/Discharge Rate. *ACS Appl. Mater. Interfaces* **2016**, *8* (51), 35342−35352.

(20) Kresse, G.; Furthmuller, J. Efficient iterative schemes for ab initio total-energy calculations using a plane-wave basis set. *Phys. Rev. B: Condens. Matter Mater. Phys.* **1996**, *54* (16), 11169−11186.

(21) Kresse, G.; Joubert, D. From ultrasoft pseudopotentials to the projector augmented-wave method. *Phys. Rev. B: Condens. Matter Mater. Phys.* **1999**, *59* (3), 1758−1775.

(22) Perdew, J. P.; Burke, K.; Ernzerhof, M. Generalized gradient approximation made simple. *Phys. Rev. Lett.* **1996**, *77* (18), 3865−3868.

(23) Heyd, J.; Scuseria, G. E.; Ernzerhof, M. Hybrid functionals based on a screened Coulomb potential. *J. Chem. Phys.* **2003**, *118* (18), 8207−8215.

(24) Monkhorst, H. J.; Pack, J. D. Special points for Brillouin-zone integrations. *Phys. Rev. B* **1976**, *13* (12), 5188−5192.

(25) Togo, A.; Oba, F.; Tanaka, I. First-principles calculations of the ferroelastic transition between rutile-type and $CaCl_2$-type SiO_2 at high pressures. *Phys. Rev. B: Condens. Matter Mater. Phys.* **2008**, *78* (13), 134106.

(26) Bucher, D.; Pierce, L. C.; McCammon, J. A.; Markwick, P. R. On the Use of Accelerated Molecular Dynamics to Enhance Configurational Sampling in Ab Initio Simulations. *J. Chem. Theory Comput.* **2011**, *7* (4), 890−897.

(27) Duerloo, K.-A. N.; Ong, M. T.; Reed, E. J. Intrinsic Piezoelectricity in Two-Dimensional Materials. *J. Phys. Chem. Lett.* **2012**, *3* (19), 2871−2876.

(28) Zhu, H.; Wang, Y.; Xiao, J.; Liu, M.; Xiong, S.; Wong, Z. J.; Ye, Z.; Ye, Y.; Yin, X.; Zhang, X. Observation of piezoelectricity in free-standing monolayer MoS_2. *Nat. Nanotechnol.* **2015**, *10* (2), 151−155.

(29) Andrew, R. C.; Mapasha, R. E.; Ukpong, A. M.; Chetty, N. Mechanical properties of graphene and boronitrene. *Phys. Rev. B: Condens. Matter Mater. Phys.* **2012**, *85* (12), 125428.

(30) Blonsky, M. N.; Zhuang, H. L.; Singh, A. K.; Hennig, R. G. Ab Initio Prediction of Piezoelectricity in Two-Dimensional Materials. *ACS Nano* **2015**, *9* (10), 9885−9891.

(31) Fei, R.; Li, W.; Li, J.; Yang, L. Giant piezoelectricity of monolayer group IV monochalcogenides: SnSe, SnS, GeSe, and GeS. *Appl. Phys. Lett.* **2015**, *107* (17), 173104.

(32) Alyörük, M. M.; Aierken, Y.; Çakır, D.; Peeters, F. M.; Sevik, C. Promising Piezoelectric Performance of Single Layer Transition-Metal Dichalcogenides and Dioxides. *J. Phys. Chem. C* **2015**, *119* (40), 23231−23237.

(33) Alyörük, M. M. Piezoelectric properties of monolayer II-VI group oxides by first-principles calculations. *Phys. Status Solidi B* **2016**, *253* (12), 2534−2539.

(34) Sevik, C.; Çakır, D.; Gülseren, O.; Peeters, F. M. Peculiar Piezoelectric Properties of Soft Two-Dimensional Materials. *J. Phys. Chem. C* **2016**, *120* (26), 13948−13953.

(35) Guo, Y.; Zhu, H.; Wang, Q. Piezoelectric Effects in Surface-Engineered Two-Dimensional Group III Nitrides. *ACS Appl. Mater. Interfaces* **2019**, *11* (1), 1033−1039.

(36) Azevedo, S.; Kaschny, J. R.; de Castilho, C. M. C.; de Brito Mota, F. Theoretical investigation of native defects in a boron nitride monolayer. *Nanotechnology* **2007**, *18* (49), 495707.

(37) Le Page, Y.; Saxe, P. Symmetry-general least-squares extraction of elastic data for strained materials fromab initiocalculations of stress. *Phys. Rev. B: Condens. Matter Mater. Phys.* **2002**, *65* (10), 104104.

(38) Ding, Y.; Wang, Y. Density Functional Theory Study of the Silicene-like SiX and XSi_3 (X = B, C, N, Al, P) Honeycomb Lattices: The Various Buckled Structures and Versatile Electronic Properties. *J. Phys. Chem. C* **2013**, *117* (35), 18266−18278.

(39) Peng, Q.; De, S. Outstanding mechanical properties of monolayer MoS_2 and its application in elastic energy storage. *Phys. Chem. Chem. Phys.* **2013**, *15* (44), 19427−19437.

(40) Guo, Y.; Zhang, C.; Zhou, J.; Wang, Q.; Jena, P. Lattice Dynamic and Instability in Pentasilicene: A Light Single-Element Ferroelectric Material With High Curie Temperature. *Phys. Rev. Appl.* **2019**, *11* (6), No. 064063.

(41) King-Smith, R. D.; Vanderbilt, D. Theory of polarization of crystalline solids. *Phys. Rev. B: Condens. Matter Mater. Phys.* **1993**, *47* (3), 1651−1654.

(42) Resta, R. Macroscopic polarization in crystalline dielectrics: the geometric phase approach. *Rev. Mod. Phys.* **1994**, *66* (3), 899−915.

(43) Dreyer, C. E.; Lyons, J. L.; Janotti, A.; Van de Walle, C. G. Band alignments and polarization properties of BN polymorphs. *Appl. Phys. Express* **2014**, *7*, No. 031001.

(44) Jia, H. J.; Mu, H. M.; Li, J. P.; Zhao, Y. Z.; Wu, Y. X.; Wang, X. C. Piezoelectric and polarized enhancement by hydrofluorination of penta-graphene. *Phys. Chem. Chem. Phys.* **2018**, *20* (41), 26288−26296.

(45) Hinchet, R.; Khan, U.; Falconi, C.; Kim, S.-W. Piezoelectric properties in two-dimensional materials: Simulations and experiments. *Mater. Today* **2018**, *21* (6), 611−630.

(46) Karbhal, I.; Devarapalli, R. R.; Debgupta, J.; Pillai, V. K.; Ajayan, P. M.; Shelke, M. V. Facile Green Synthesis of BCN Nanosheets as High-Performance Electrode Material for Electrochemical Energy Storage. *Chem. - Eur. J.* **2016**, *22* (21), 7134−7140.

(47) Beniwal, S.; Hooper, J.; Miller, D. P.; Costa, P. S.; Chen, G.; Liu, S. Y.; Dowben, P. A.; Sykes, E. C.; Zurek, E.; Enders, A. Graphene-like Boron-Carbon-Nitrogen Monolayers. *ACS Nano* **2017**, *11* (3), 2486−2493.